Proceedings of the ASME 2021
International Mechanical Engineering Congress and Exposition
IMECE2021
November 1-5, 2021, Virtual, Online

IMECE2021-71751

Power Estimation of an Experimental Ocean Current Turbine Based on the Conformal Mapping and Blade Element Momentum Theory

S. Sadeqi
University of New Orleans
New Orleans, LA

N. Xiros
University of New Orleans
New Orleans, LA

E. Aktosun
University of New Orleans
New Orleans, LA

J. VanZwieten
Florida Atlantic University
Boca Raton, FL

C. Sultan
Virginia Tech.
Blacksburg, VA

J. Ioup
University of New Orleans
New Orleans, LA

S. Rouhi
University of New Orleans
New Orleans, LA

ABSTRACT

Conformal mapping techniques have been used in many applications in the two-dimensional environments of engineering and physics, especially in the two-dimensional incompressible flow field that was introduced by Prandtl and Tietjens. These methods show reasonable results in the case of comprehensive analysis of the local coefficients of complex airfoils. The mathematical form of conformal mapping always locally preserves angles of the complex functions but it may change the length of the complex model. This research is based on the design of turbine blades as hydrofoils divided into different individual hydrofoils with decreasing thickness from root to tip. The geometric shapes of these hydrofoils come from the original FX77W121 airfoil shape and from interpolating between the FX77W121, FX77W153, and FX77W258 airfoil shapes. The last three digits of this airfoil family approximate the thickness ratio times 1000 (FX77153 => 15.3 % thickness ratio). Of the different airfoil shapes specified for the optimal rotor, there are 23 unique shapes. [15,16,17,18,19,20,21,22,24,25,28]This study describes the advantage of using at least one complex variable technique of transformation conformal mapping in two dimensions. Conformal mapping techniques are used to form a database for sectional lift and drag coefficients based on turbine blade design to be used in Blade Element Momentum (BEM) theory to predict the performance of a three bladed single rotor horizontal axis ocean current turbine (1.6-meter diameter) by considering the characteristics of the sea-water. In addition, by considering the fact that in the real ocean, the underwater ocean current turbines encounter different velocities, the maximum brake power will be investigated for different incoming current velocities. The conformal mapping technique is used to calculate the local lift coefficients of different hydrofoils with respect to different angles of attack: -180≤AOA≤+180. These results will be compared to those from other methods obtained recently by our research group. This method considers the potential flow analysis module that follows a higher-order panel method based on the geometric properties of each hydrofoil cross section. The velocity and pressure fields are obtained directly by the applications of Bernoulli's principle, then the lift coefficients are calculated from the results of the integration of the pressure field along the hydrofoil surface for any angle of attack. Ultimately, the results of this research will be used for further investigation of the design and construction of a small-scale experimental ocean current turbine to be tested in the towing tank at the University of New Orleans.

Keywords: Conformal Mapping, Joukowsky, Prandtl, Incompressible Flow, Local Coefficient, Drag Coefficient, Lift Coefficient, Blade Element Momentum Theory, Complex Function, Hydrofoil Design, Three-Bladed Rotor, Ocean Current Turbine, Efficiency, Angle of Attack, Axial Induction Factor, Tangential Induction Factor, Bernoulli's Principle, Pressure Field, Incoming Flow Velocity.

NOMENCLATURE

Place nomenclature section, if needed, here. Nomenclature should be given in a column, like this:

A	Cross Sectional Area
ρ	Density of the Sea-water
U	Flow Velocity
a	Axial Flow Induction Factor
a'	Tangential Flow Induction Factor

Ω	Angular Velocity
r	Radius of the Actuator disc/ The Local Radius on the Rotor
R	Rotor Radius
V_{rel}	Resultant Velocity
c	Chord Length
N	Number of Blades
β	Set Pitch Angle
α	Angle of Attack (AOA)
φ	Local Inflow Angle
C_l	Lift Coefficient
C_d	Drag Coefficient
δL	Cross Sectional Lift Force
δD	Cross Sectional Drag Force
Q	Torque
P	Power
T	Thrust
F_n	Loading on Each Blade in Axial Direction
F_t	Loading on Each Blade in Tangential Direction
C_p	Pressure Coefficient
C_P	Power Coefficient
TSR	Tip Speed Ratio

1. INTRODUCTION

Generating clean energy from renewable resources is an important theme for scientists. It is not easy to harness the energy from uncontrollable resources such as oceans. It is crucial to find the most appropriate and safe methods to restrain and use its clean and sustainable energy. One of the best methods to harness the energy from the ocean is to implement moored Ocean Current Turbines (OCT) to generate electricity. Performance analysis of the turbine based on simulation will help guide further research such as constructing small-scale OCTs in laboratories and then later building full size OCTs for the oceans. In this research, we implemented conformal mapping to design hydrofoils for rotor blades. The hydrodynamic forces and the related coefficients of the mapped hydrofoils is calculated by integrating the pressure forces around the hydrofoils. The next step is to transfer these initial data to the in-house Blade Element Momentum Theory (BEM) to analyze the performance of the turbine. Based on the results of the BEM theory, the torque, thrust and power of the turbine will be determined by considering the direct effects of the axial and tangential induction factors . We will use these data as a model to build an experimental scale ocean current turbine that will be tested at the University of New Orleans Towing Tank. The results of the simulation and the towing tank experiment will be compared.

In 2016 the World Total Primary Energy Supply (TPES) by fuel was Oil, 31.9%; Coal, 27.1%; Natural Gas, 22.1%; Biofuels and Waste, 9.8%; Nuclear, 4.9%; Hydro, 2.5%; and others renewable resources 1.7%. It is clear that the TPES by clean renewable energy is very small and needs to be developed. [7] Bobby Zarubin noted that the best sites to harness the ocean current energy are between islands where the tidal currents are the strongest or locations in the oceans where the temperature difference is about 20℃ between the warm surface water and the cold deep water.

The length of the real turbine blades should be at least 20 meters. [8] Ilan Robin el al. describe the minimum current velocity needed to rotate the blades of the turbine. They found a novel method to model the fluid-structure interaction on tidal vertical and horizontal turbines. [9] Matt Edmunds el al. showed a new generalized actuator disc model based on the CFD method that obtained the best accuracy for the horizontal axis turbines. [10] Lundin in his research found out it is possible to build small energy conversion units for very low current speed by implementing an accurate system efficiency. Also, he mentioned the role of the proper material in describing the results of real-world experiments. [11] Uihlein and Magagna noted that the installation, operation and maintenance of renewable ocean energy devices are extremely expensive. A promising improvement option is the use of modelling tools. [12] The results of the simulation by Maimun and Aljen show that a turbine is able to produce about 24 KW at a flow speed of 2m/s. They found that by creating a farm of these turbines in an area of 370 m X 10 m, they were able to produce about 280- 290 KW. Implementing these farms will help to save fuel and also have a direct effect in the reduction of CO_2 emissions. [13] In this research conformal mapping technique is used to form a database for sectional drag and lift coefficients based on turbine blade design characteristics. These are going to be used in Blade Element Momentum (BEM) theory to predict the performance of a three bladed single rotor horizontal axis ocean current turbine by considering the characteristics of the ocean-water.

2. MATERIALS AND METHODS

2.1 Conformal Mapping Technique [1]

The conformal mapping technique is one of the most powerful and effective methods to find solutions of the complicated Laplace equation that is often used in aerodynamics and fluid mechanics.

The explicit Poisson integral formula is able to solve and provide solutions to the Laplace equation with Dirichlet boundary conditions. Consider a unit circular disc ($r = 1$) based on the following equations:[2, Theorem 4.6]:

$$u(r,\theta) = h(\theta) \qquad (1)$$

where

$$h(x,y) = h(\cos\theta\,, \sin\theta) \equiv h(\theta), \qquad -\pi < \theta \leq \pi. \qquad (2)$$

$$(r,\theta) = \frac{1}{2\pi}\int_{-\pi}^{+\pi} h(\phi)\,\frac{1-r^2}{1+r^2-2r\cos(\theta-\phi)}\,d\phi \qquad (3)$$

For more sophisticated boundary condition problems, we need to transform these equations by changing variables.

Consider a complex analytical function

$$\chi = f(z) \qquad (4)$$

where

$$\chi = \xi + i\,\eta \qquad (5)$$

and

$$f(z) = p(x,y) + i\,q(x,y) \qquad (6)$$

so,

$$\xi + i\,\eta = p(x,y) + i\,q(x,y). \qquad (7)$$

As a mapping function, we are going to map a point $z = x + iy$ which belongs to the domain Ω, $\Omega \subset \mathbb{C}$. ($z \in \Omega$) to a point like $\chi = \xi + i\,\eta$ which is belonging to the other subset of the $\mathbb{C}$ which is the image domain $D = f(\Omega) \subset \mathbb{C}$. In most of the well-known problems in fluid mechanics, the image domain is defined to be the unit circle. One of the most important requirements for mapping is that the analytic mapping (7) must be invertible. Conformal mapping always preserves angles but nor necessarily curvatures. In the most simple definition, if $\chi = f(z)$ is a complex analytic function and its first derivative exists and is non-zero ($f'(z) = 0$), then f defines a conformal map. [1, Theorem 5.[12]

The noble Russian scientist Nikolai Joukowsky developed a conformal mapping technique to study the flows around wings of an airplane, which is known as the Joukowsky map. In his study,

$$\xi = \frac{1}{2}\left(z + \frac{1}{z}\right) \qquad (8)$$

Since,

$$\frac{d\xi}{dz} = \frac{1}{2}\left(1 - \frac{1}{z^2}\right) = 0 \qquad (9)$$

if and only if $z = \pm 1$, which are the critical points.

By considering that the point $z = 0$ is not defined in the domain, then the Joukowsky map is always conformal except at the following points: $(z = \pm 1, 0)$.

Applying the Joukowsky conformal mapping technique to an off-center circular disc will produce an airfoil. It is obvious that flow distribution around new airfoil can be obtained form the fluid motion around the initial circular disc. Let's assume the initial map to be

$$\omega = \alpha z + \beta \qquad (10)$$

This changes the radius of the unit circle ($|z| \ll 1$) to a new disc with radius α and center β.

$$|\omega - \beta| \ll |\alpha| \qquad (11)$$

The component α is responsible for the circulation, and the streamlines around new disc will be an angle $\Phi = ph\ \alpha$ with the horizontal. [1]

Now, by applying the Joukowsky transformation:

$$\xi = \frac{1}{2}\left(\omega + \frac{1}{\omega}\right) = \frac{1}{2}\left(\alpha z + \beta + \frac{1}{\alpha z + \beta}\right) \qquad (12)$$

$$\Theta(\xi) = \frac{\xi - \beta - \sqrt{\xi^2 - 1}}{\alpha} + \frac{\alpha\left(\xi - \beta - \sqrt{\xi^2 - 1}\right)}{\beta^2 + 1 - 2\beta\xi} \qquad (13)$$

and the complex potential flow function around a disc equation as:

$$\chi(z) = z + \frac{1}{z} = \left(x + \frac{x}{x^2 + y^2}\right) + i\left(y - \frac{y}{x^2 + y^2}\right) \qquad (14)$$

By substituting equation 13 into equation 14, we get:

$$\Theta(\xi) = \frac{\xi - \beta - \sqrt{\xi^2 - 1}}{\alpha} + \frac{\alpha(\xi - \beta - \sqrt{\xi^2 - 1})}{\beta^2 + 1 - 2\beta\xi} \qquad (15)$$

By substituting ξ with $e^{i\varphi\xi}$, streamlines will be produced around the airfoil based on the angle of attack φ to the horizontal flow.

$$\Theta\left(e^{i\varphi\xi}\right) = \frac{e^{i\varphi\xi} - \beta - \sqrt{e^{i\varphi\xi^2} - 1}}{\alpha} + \frac{\alpha(e^{i\varphi\xi} - \beta - \sqrt{e^{i\varphi\xi^2} - 1})}{\beta^2 + 1 - 2\beta e^{i\varphi\xi}} \qquad (16)$$

Lift and Drag Coefficients of the Joukowsky Airfoil [3] will be calculated by integrating the horizontal and vertical components of the pressure field around the mapped airfoil, the hydrodynamic forces can be computed.

$$F_d = \int p(\vec{r})\hat{n}_x(\vec{r})\overrightarrow{dr}^{airfoil} = -\int_0^{2\pi} p\big(z(\theta)\big)\, im\left(\frac{\partial z}{\partial \theta}\right) d\theta \qquad (17)$$

$$F_l = \int p(\vec{r})\hat{n}_y(\vec{r})\overrightarrow{dr}^{airfoil} = \int_0^{2\pi} p\big(z(\theta)\big)\, re\left(\frac{\partial z}{\partial \theta}\right) d\theta \qquad (18)$$

2.2 Blade Element Momentum Theory (BEM) [4]

Nowadays, the most appropriate method to analyze and predict the performance of wind or current turbines is Blade Element Momentum theory (BEM) by Glauert (1953). This method is straightforward to program and implement on the computer. Also, it considers most of the physical conditions of the flow and rotor blades.

To briefly look into the BEM theory, assume the simple condition of a fluid flow that is acting at a right angle to the rotor blade. The sum of the flow speed vector, the blade velocity Ωr and the induced velocity from the pressure field give the relative flow field. The angle between the airfoil chord line and the relative velocity indicates the angle of attack (α). The dimensionless hydrodynamics coefficients (Lift C_l and Drag C_d coefficients) will be calculated locally from tabulated airfoil information by considering the angle of attack, airfoil type that was obtained by the conformal mapping technique, and the related Reynolds number.

The axial load and torque equations are shown in the following equations, respectively:

$$\frac{dT}{dr} = N_b F_n = \frac{1}{2\rho c N_b V_{rel}^2} . C_n \qquad (19)$$

$$\frac{dQ}{dr} = r N_b F_t = \frac{1}{2\rho c r N_b V_{rel}^2} . C_t \qquad (20)$$

where c is the blade chord length, N_b is the number of blades, V_{rel} indicates the relative velocity, F_n shows the loading on each blade in axial direction, F_t indicates the loading on each blade in the tangential direction. C_n and C_t are the corresponding 2D force coefficients that are defined as:

$$C_n = \frac{F_n}{\frac{1}{2\rho c V_{rel}^2}} \qquad (21)$$

$$C_t = \frac{F_t}{\frac{1}{2\rho c V_{rel}^2}} \qquad (22)$$

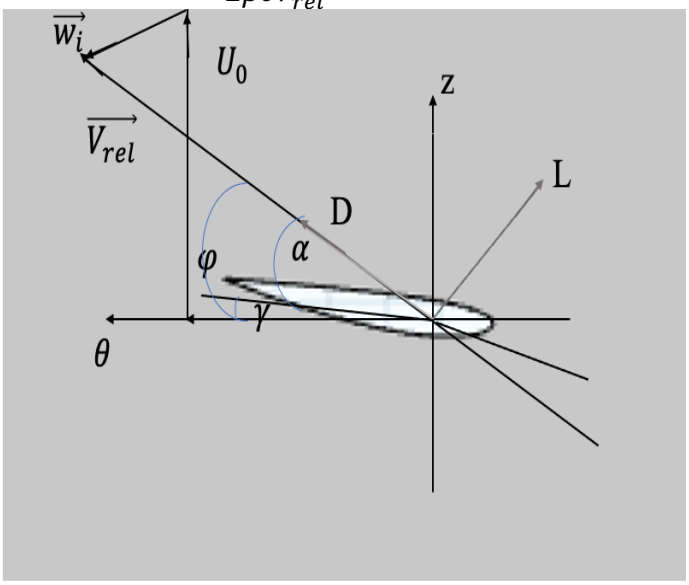

FIGURE 1: BEM Vector Presentation

Note that the lift and drag coefficients made up the following force coefficients.

$$C_n = C_l \cos\varphi + C_d \sin\varphi \qquad (23)$$

$$C_t = C_l \sin\varphi - C_d \cos\varphi \qquad (24)$$

where φ is the flow angle which depends directly on the local airfoil shape. Suppose the sum of the local twist angle and pitch angle of the rotor blade is γ, then the corresponding angle of attack is

$$\alpha = \varphi - \gamma \qquad (25)$$

From figure 1 we can conclude that:

$$\sin\varphi = \frac{U_0(1-a)}{V_{rel}} \qquad (26)$$

$$\cos\varphi = \frac{\Omega r(1-a')}{V_{rel}} \qquad (27)$$

Where a and a' denote the axial and tangential induction factors. Then,

$$V_{rel}^2 = \frac{U_0^2(1-a)^2}{\sin\varphi^2} = \frac{U_0(1-a)\Omega r(1+a')}{\sin\varphi\ \cos\varphi} \qquad (28)$$

Now, by substituting equation 26 into equations 17 and 18, we will obtain:

$$\frac{dT}{dr} = N_b F_n = \frac{\rho c N_b U_0^2(1-a)^2}{2(\sin\varphi)^2} . C_n \qquad (29)$$

$$\frac{dQ}{dr} = r N_b F_t = \frac{\rho c N_b U_0(1-\mathrm{a})\Omega r^2(1+a')}{2\sin\varphi\ \cos\varphi} . C_t \qquad (30)$$

Then, according to the result of the axial momentum theory, the axial load and axial torque are obtained as:

$$\frac{dT}{dr} = \rho(U_0 - u_1)2\pi r u_R = 4\pi\rho r U_0^2 a(1-a) \qquad (31)$$

$$\frac{dQ}{dr} = \rho r u_\theta 2\pi r u_R = 4\pi\rho r^3 \Omega U_0 a'(1-a) \qquad (32)$$

where $u_R = U_0(1-a)$ is the axial velocity of the rotor, $u_1 = U_0(1-2a)$ is the axial velocity in the wake and, $u_\theta = 2r\Omega a'$ indicates the induced tangential velocity downstream of the rotor.

Combining the following equations and performing some algebraic manipulations, we have:

$$a = \frac{1}{\frac{4(\sin\varphi)^2}{\sigma C_n} + 1} \qquad (33)$$

$$a' = \frac{1}{\frac{4\sin\varphi\cos\varphi}{\sigma C_t} - 1} \qquad (34)$$

where σ denotes the local solidity. These two expressions are the most important equations of the BEM theory. Finally, the axial and tangential induction factors will be calculated iteratively.

3. RESULTS AND DISCUSSION

3.1 Conformal Mapping

The first part of this research focused on creating airfoils by using conformal mapping. Figures 2, 3 and 4 show the potential flow around a circle with its center located at -0.1+0.1i, potential flow around the mapped airfoil with angle of attack is $\varphi = 0°$,

tail angle as 0°, and pressure distribution coefficient vs. $\frac{x}{c}$ of the mapped airfoil (where the number of points for pressure distribution is defined to be 100 points. At $\frac{x}{c} = 0.3276$, the pressure coefficient is calculated as $C_p = -1.047$.

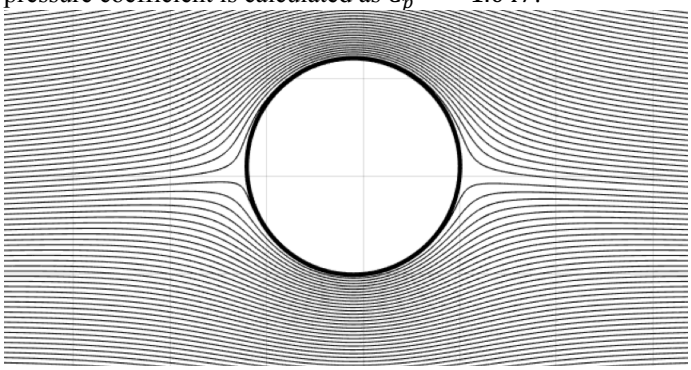

FIGURE 2: Potential Flow around the circle

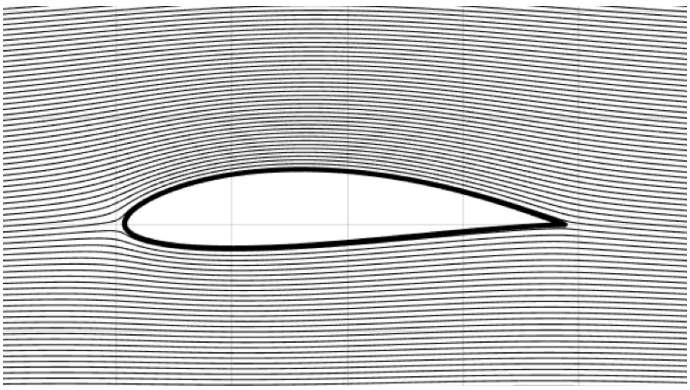

FIGURE 3: Potential Flow around the mapped airfoil

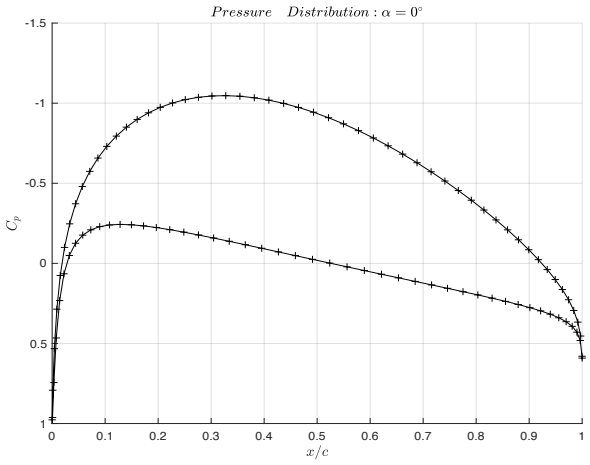

FIGURE 4: Pressure Distribution of the mapped airfoil

Changing the center of the default circle from -0.1+0.1i to 0.1+0.2i,new results are as follows. Figure 5 shows the potential flow around the circle. The potential flow around the new mapped airfoil is indicated in figure 7. Figure 8 illustrates the pressure coefficients vs. $\frac{x}{c}$. . It is important that at $\frac{x}{c} = 0.3872$, the pressure coefficient is calculated as $C_p = -1.637$. As before, the angle of attack and tail angle are considered to be 0°, and the number of points for pressure distribution is 100 points.

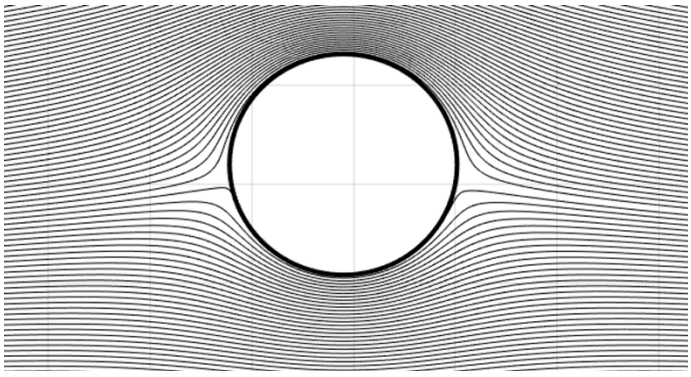

FIGURE 5: Potential Flow around the circle with different center

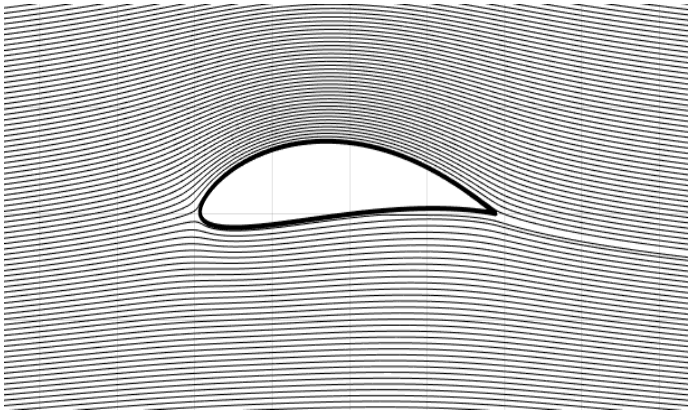

FIGURE 6: Potential Flow around the mapped airfoil with different center

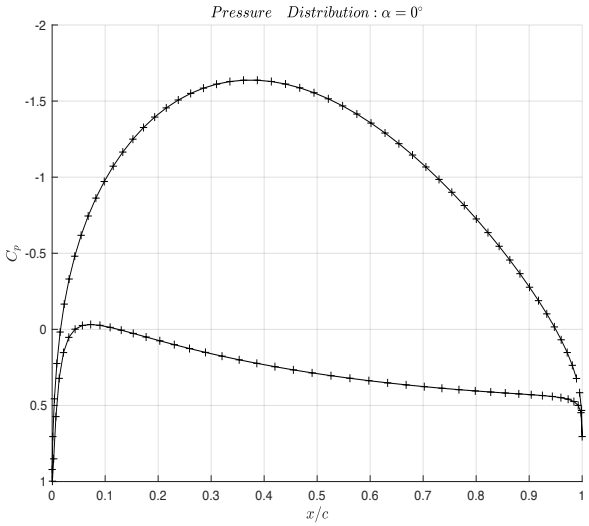

FIGURE 7: Pressure Distribution of the mapped airfoil

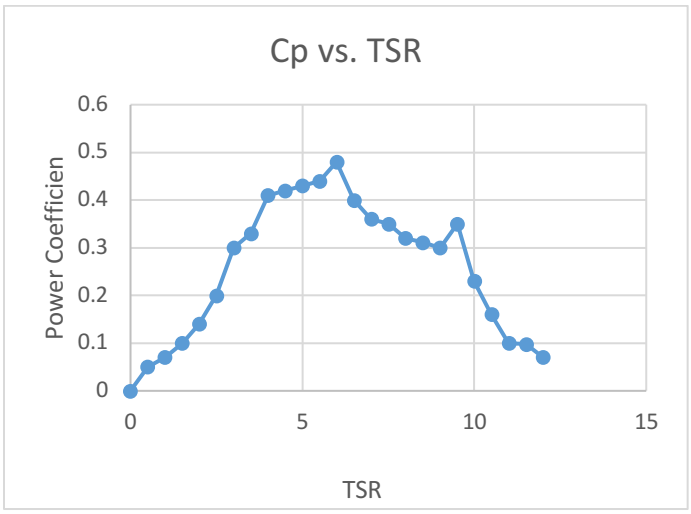

FIGURE 8: Power Coefficient vs. TSR

3.2 Blade Element Momentum Theory

After designing appropriate airfoils and obtaining their related hydrodynamics coefficient, we transferred these data to be implemented in our in-house BEM code to analyze the rotor performance of a turbine which uses these airfoils.

3.2.1 The Optimum Power Coefficient:

We considered that the rotor to be operating at its maximum power performance. Using this maximum power, the optimum power coefficient will be determined.
Equation 33 shows how to calculate the power based on the load torque.

$$P = \Omega Q = \Omega \int_0^R 2\pi r^2 \rho u_r u_\theta dr = 4\pi\rho\Omega^2 R^4 U_0 \int_0^1 a'(1 - a)\mu^3 d\mu \qquad (33)$$

In the dimensionless form the following equation will convert to the:

$$C_p = \frac{P}{1/2\,\rho A U_0^3} = 8\lambda^2 \int_0^1 a'(1-a)\mu^3 d\mu \qquad (34)$$

where $\lambda = \frac{\Omega R}{U_0}$ denotes the tip speed ratio, and $\mu = \frac{r}{R}$ shows the dimensionless spanwise coordinate. Figure 8 shows how the dimensionless power coefficient changes with increasing tip speed ratio (TSR). This figure shows that the turbine reaches its maximum power coefficient of 0.482 at TSR=6.

Figure 9 shows the power coefficient vs. TSR for an ocean current turbine with a 3.0 m diameter 3-bladed rotor by two different methods: BEM (blue) and computational Fluid Dynamics (CFD) (red) based on the RANS (Reynolds Averaged Navier-Stokes) equation and shear stress transport provided in [5]. The CFD results indicate that the turbine will obtain its maximum coefficient of power of 0.4642 at TSR=6. Our results (BEM) show good agreement with the results of [5]. The difference between the two results is less than 0.019.

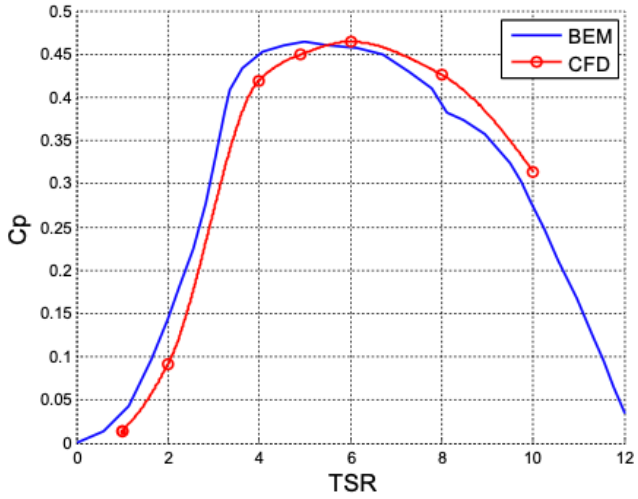

FIGURE 9: Power Coefficient vs. TSR [4]

The inflow angle is the angle between the rotor blade axis and the flow stream direction. Figure 10 shows that by increasing $\mu = \frac{r}{R}$, the inflow angle decreases. This result shows reasonable

agreement with the results for inflow angle provided by [5]. The maximum inflow angle is around $\phi_0 = 36.68°$.

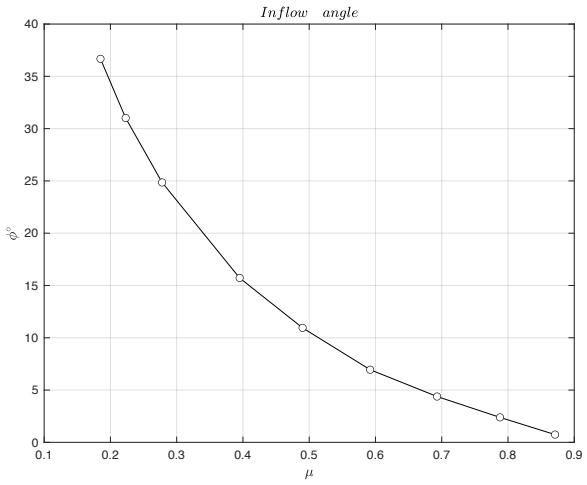

FIGURE 10: Inflow angle vs. $\mu = \frac{r}{R}$

Obtaining the most accurate axial and tangential induction factors are the most important achievements of the BEM theory. Having accurate axial and tangential induction factors is necessary to continue the performance analysis of the turbine and determine the optimum power, thrust and torque. Figure 11 shows the changing axial (blue) and tangential (red) induction factors by increasing μ. This result is in good agreement with the results of [6] which are shown in figure 12.

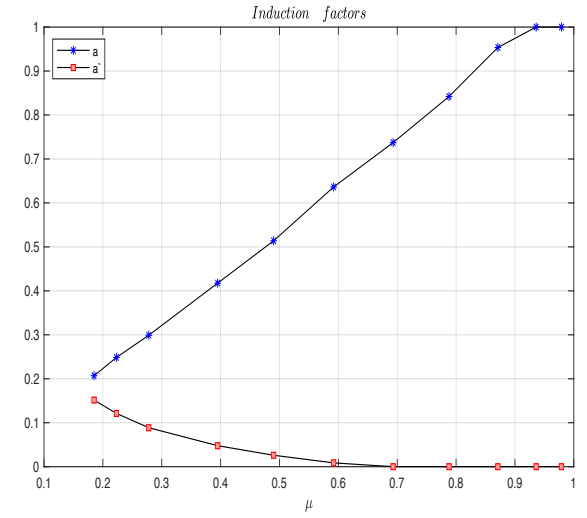

FIGURE11: Axial and Tangential Induction Factors vs. $\mu = \frac{r}{R}$

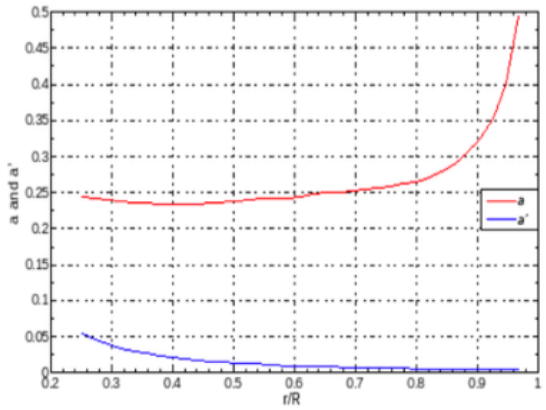

FIGURE 12: Axial and Tangential Induction Factors vs. $\mu = \frac{r}{R}$ [5]

Figures 13, 14 and 15 show the differential thrust, torque and power vs. $\mu = \frac{r}{R}$, given directly from the BEM code. Based on figure 13, the maximum differential thrust occurs at $\mu = 0.592 \cong 0.6$, the maximum differential thrust is 1166 N. The minimum thrust is obtained for $\mu >= 0.937$ which is 1 N.

Figure 14 shows the changes in the differential torque produced by increasing μ. From this figure, we can conclude that when $0.278 \leq \mu \leq 0.5$, the maximum differential load torque is observed, about $102.3\ N \leq Q \leq 105.3\ N$. The minimum torque is obtained at $\mu = 0.871$.

Figure 15 shows that, similar to the differential torque, the maximum differential power is obtained when $0.278 \leq \mu \leq 0.5$. The maximum differential power is $511.7\ W \leq Q \leq 526.5\ W$. The results for the differential toque and differential power agree with each other. These results also show good agreement with those for the differential thrust, torque and power of the research given in [6], and the behaviors follow the same trends. The only slight differences are that the maximum thrust is located at $\mu = 0.9$ and their maximum differential torque and power is located at $\mu = 0.8$.

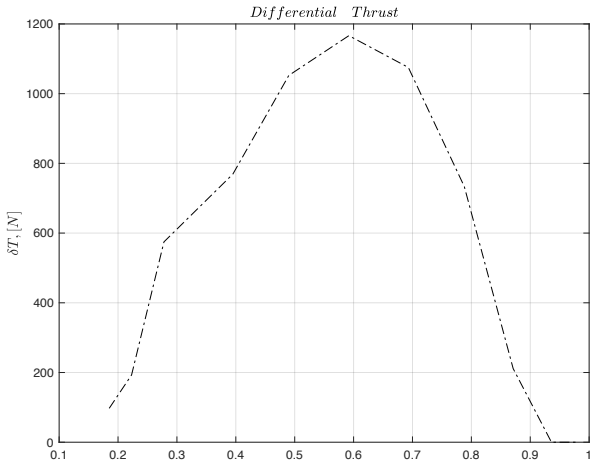

FIGURE 13: Differential Thrust vs. $\mu = \frac{r}{R}$

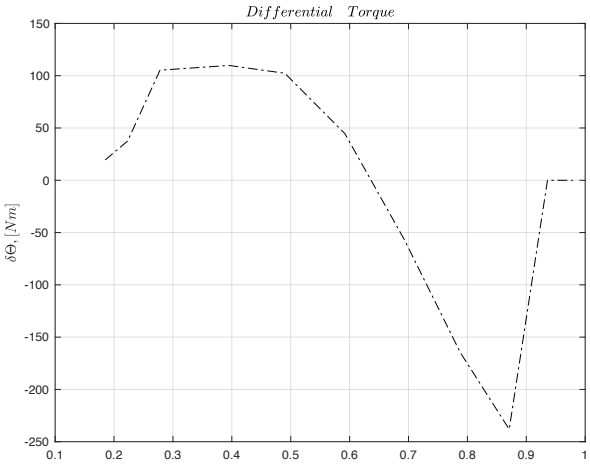

FIGURE 14: Differential Torque vs. $\mu = \frac{r}{R}$

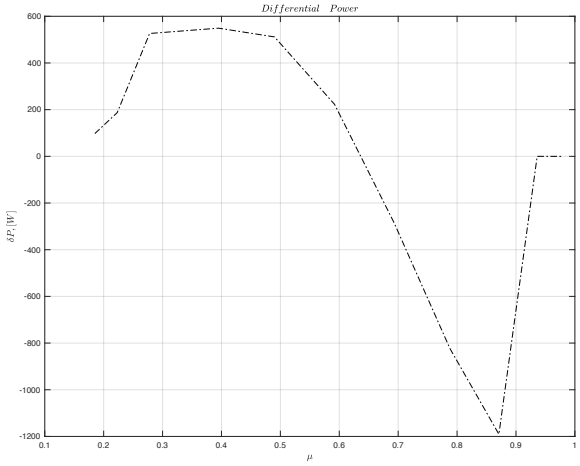

FIGURE 15: Differential Power vs. $\mu = \frac{r}{R}$

4. CONCLUSION

In this research, the Joukowsky conformal mapping technique was applied to the unit circle to create appropriate hydrofoils. These hydrofoils were used to generate the blades of an ocean current turbine model. We have developed a Blade Element Momentum Theory code to analyze the performance of the above-mentioned turbine by considering hydrodynamic forces and coefficients. . The information for the blades was used by the conformal mapping technique. The axial and tangential induction factors, the spanwise contributions of differential torque thrust and power show good agreement with similar data reported in the literature.

ACKNOWLEDGEMENTS

The authors would like to thank the National Science Foundation (NSF) and specifically the Energy, Power, Control and Networks (EPCN) program for their valuable ongoing support in this research within the framework of grant ECCS-1809182 'Collaborative Research: Design and Control of Networked Offshore Hydrokinetic Power-Plants with Energy Storage'.

REFERENCES

[1] Olver, P.J., r, *Complex Analysis and Conformal Mapping, University of Minnesota, 2020*

[2] Olver, P.J., *Introduction to Partial Differential Equations, Undergraduate Text in Mathematics, Springer-Verlag, New York.*

[3] Paul Nadan, Sean Szymanski, Colvin Chapman, *Airfoil Modeling, May 2018*

[4] Sornson, Jens, *General Momentum Theory for Horizontal Axis Wind Turbines, 2016*

[5] Wenlong Tian, James VanZwieten, Parakram Pyakurel, Yanjun Li, *Influence of Yaw Angle and Turbulence Intensity on the Performance of a 20 kw in-stream Hydrokinetic Turbine, Energy Journal, 3 June 2016*

[6] Aerodynamic Performance, *University of Notre Dame, AME, 40530.*

[7] De Gruyter, S*tate-of-the-are of MW-level capacity oceaninc current turbine, Published online: August 21, 2020, https://www.degruyter.com/document/doi/10.1515/nleng-2020-0022/html*

[8] Bobby Zarubin, *Ocean Current Energy: Underwater Turbines, Stanford University, January, 24, 2015*

[9] Robin,I.;Bennis,A.-C.; Dauvin, *J.-C. 3D Simulation with Flow-Induced Rotation for Non-Deformable Tidal Turbines. J. Mar. Sci. Eng.* ***2021****, 9, 250. https:// doi.org/10.3390/jmse9030250*

[10] Edmunds Matt, Williams Alison, Masters Ian, Banerjee Arindam, VanZwieten, *A spatially nonlinear generalized actuator disc model for the simulation of horizontal wind and tidal turbines, Energy Journal, 23 December 2019*

[11] Staffan Lundin, *Marine Current Energy Conversion, UPPSALA university, Summary of the Dissertation, online: http://www.diva-portal.org/smash/get/diva2:911949/FULLTEXT01.pdf*

[12] Uihlein Andreas, Magagna Davide, *Wave and Tidal current energy- A Review of the Current state of Research Beyond Technology, Renewable and Sustainable Enegy Reviews Journal, May 2016, Pages 1070-1081*

[13] Maimun Adi, Salem Suof Aljen Atef, *The Drag Marin Vertical Axis Current Turbine to Assist in the Electrification of Offshore Platforms, Offshore Technology Conference Asia, Kuala Lumpur, Malaysia, November 2020*

[14] Burton, Tony, *Wind Energy Handbook*, *Wiley, 2011*

[15] James H. VanZwieten, *Report, SNMREC Rotor Blade Design and Predicted Performance.*

[16]James H. VanZwieten , Parakram Pyakurel , Tri Ngo , Cornel Sultan , Nikolaos I. Xiros , *An assessment of using variable*

blade pitch for moored ocean current turbine flight control, International Journal Of Marine Energy (2016)16-26
[17] C.M. Oster, (2010) *"Optimization of a Hydrodynamic Rotor Blade", Summer Internship Final Report, COET (SNMREC), August*
[18] James H. VanZwieten, Jr., Nicolas Vanrietvelde, and Basil L. Hacker, *Student Member, IEEE, Numerical Simulation of an Experimental Ocean Current Turbine.*
[19] Duerr AES, Dhanak MR. *Hydrodynamic Power Resource Assessment of the Florida Current, In: MTS/IEEE ocean conference 2010. Seattle; September 20-23,2010.*
[20] Wenlong Tian , James H. VanZwieten , Parakram Pyakurel , Yanjun Li, *Influences of yaw angle and turbulence intensity on the performance of a 20 kW in-stream hydrokinetic turbine, Energy Journal, Available online 3 June 2016.*
[21] Michael Borghi, Fumbi Kolawole, Sathya Gangadharan, Willoam Engblom, James H. VanZwieten, Gabriel Alsenas, William Baxley, Shirely Ravenna, *Design, Fabrication and Installation of a Hydrodynamic Rotor for a Small-Scale Experimental Ocean Current Turbine*.
[22] James H. VanZwieten, Carey Oster, Alana Duerr, *Design ana Analysis of a Rotor Blade Optimized for Extracting Energy from the Florida Current.*
[23] JavaFoil *User's Guide, Martin Hepperle, 22-Dec-2017*
[24] S. Rouhi, N. Xiros, S. Sadeqi, J. Ioup, J. VanZwieten, C. Sultan, *"CFD Validation of the Thermodynamic Model of a Compressed Gaseous Hydrogen Storage Tank". American Society of Thermal and Fluids Engineers. (2021) TFEC-2020-36525*
[25] S. Sadeqi, N. Xiros, S. Rouhi, J. Ioup, J. VanZwieten, C. Sultan, *"Wavelet Transform Analysis Applied to Incompressible Flow Field About a Solid Cylinder". American Society of Thermal and Fluids Engineers. (2021) TFEC-2020-36526*
[26] S. Rouhi, S. Sadeqi, N. Xiros, J. Ioup, *"CFD Analysis of Filling Process for a Hydrogen Energy Storage System". American Society of Thermal and Fluids Engineers. (2020) TFEC-2020- 32066*
[27] S. Yoshida, F. Miura, T. Sasaki, S. Rouhi, *"Optical Analysis of Residual Stress with Minimum Invasion". The Society for Experimental Mechanic (SEM) annual/volume 8/ paper 141. (2017)*
[28] S. Sadeqi, N. Xiros, S. Rouhi, J.Ioup, J. VanZwieten, C. Sultan, Numeri Numerical Investigation of an Experimental Ocean Current Turbine Based on Conformal Mapping Techniques and Blade Element Momentum Theory, OMAE2021-63010